

NASA TM X-455

Facility Form 602

N66 33306

(ACCESSION NUMBER)

42

(INDEX)

TMX-455

(BASE OR TMX OR AD NUMBER)

(GRADE)

(CODE)

(CATEGORY)



(Memo) 596  
Copy

NASA TM X-455

GPO PRICE \$

CFSTI PRICE(S) \$

Hard copy (HC)

Microfiche (MF)

# 653 July 65

# TECHNICAL MEMORANDUM

X-455

WIND-TUNNEL INVESTIGATION AT A MACH NUMBER OF 2.91  
OF STABILITY AND CONTROL CHARACTERISTICS OF  
THREE LIFTING REENTRY CONFIGURATIONS AT  
ANGLES OF ATTACK UP TO 90°

By John E. Grimaud

Langley Research Center  
Langley Field, Va.

DECLASSIFIED- AUTHORITY  
US: 1286 DROBKA TO LEBOW  
MEMO DATED

6/8/66 Declassified by authority of NASA  
Classification Change Notices No. 62  
Dated \*\* 6/29/66

NATIONAL AERONAUTICS AND SPACE ADMINISTRATION  
WASHINGTON

March 1961

[REDACTED]

NATIONAL AERONAUTICS AND SPACE ADMINISTRATION

TECHNICAL MEMORANDUM X-455

WIND-TUNNEL INVESTIGATION AT A MACH NUMBER OF 2.91  
OF STABILITY AND CONTROL CHARACTERISTICS OF  
THREE LIFTING REENTRY CONFIGURATIONS AT  
ANGLES OF ATTACK UP TO  $90^{\circ}$ \*

By John E. Grimaud

SUMMARY

73306

An investigation has been conducted in the Langley 9-inch supersonic tunnel at a Mach number of 2.91 to determine the stability and control characteristics of models of three lifting reentry configurations. These configurations were of the type that would reenter the earth's atmosphere near maximum lift. Longitudinal control for the models was provided by flaps which extended beyond the trailing edge of each wing. Directional stability was provided by fins located at the tip of each wing. One model was tested over an angle-of-attack range from  $-4^{\circ}$  to  $90^{\circ}$  with flap deflections ranging from  $0^{\circ}$  to  $\pm 70^{\circ}$ . This model was also tested over a combined angle-of-attack and angle-of-sideslip range with angles of attack up to  $51^{\circ}$ . Tests on the other two models were restricted to an angle-of-attack range near maximum lift for flap deflections ranging from  $0^{\circ}$  to  $-50^{\circ}$ .

Results indicated that one model could be trimmed and was longitudinally stable over an angle-of-attack range up to  $41^{\circ}$  with the center of gravity located at 58 percent of the body length. The trim-lift-coefficient values for this model ranged from 0.13 at an angle of attack of  $-4^{\circ}$  with a flap deflection of  $50^{\circ}$  to 0.63 at an angle of attack of  $41^{\circ}$  with flap deflections of  $-50^{\circ}$  and  $-70^{\circ}$ . This model was also directionally stable over a combined angle-of-attack and angle-of-sideslip range with angles of attack up to  $50^{\circ}$ .

Author

---

\*Title, Unclassified.

[REDACTED]

## INTRODUCTION

An investigation is being conducted by the National Aeronautics and Space Administration to provide information on the stability and control characteristics from low subsonic to hypersonic speeds of some configurations suitable for a lifting reentry into the earth's atmosphere. Results of different phases of this investigation are presented in references 1 to 7. The tests of reference 1 were conducted at a Mach number of 2.91 to determine the stability and control characteristics of four triangular-wing configurations which might reenter the earth's atmosphere at maximum lift or at an angle of attack of  $90^\circ$ . The present investigation used three configurations which were modified versions of model A of reference 1. Modifications consisted of beveling the wings in front of the apertures which were ahead of the flaps, deflecting the nose portion of the model, increasing the flap and tip-fin areas, and varying the tip-fin roll-out and toe-in angles. The purpose of this investigation was to determine the effect of these modifications on the stability and control characteristics of the configurations near maximum lift and to develop a configuration which could be trimmed at a large lift coefficient. The tests were conducted at a free-stream Mach number of 2.91. One model was tested over an angle-of-attack range from  $0^\circ$  to  $90^\circ$  with flap deflections up to  $\pm 70^\circ$  and over a combined angle-of-attack and angle-of-sideslip range with angles of attack to as high as  $51^\circ$ . The tests on the other two models were restricted to an angle-of-attack range near maximum lift with a flap-deflection range from  $0^\circ$  to  $-50^\circ$ .

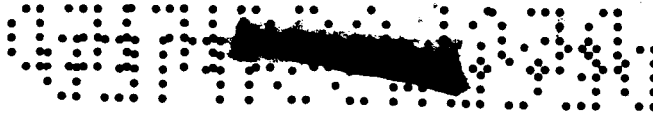
## SYMBOLS

The force and moment coefficient data are given with respect to the stability-axis system. The origin of the axes was located to correspond to a longitudinal center-of-gravity position at 58 percent of the body length for each model.

- b            wing span, in.
- c            root chord, in.
- $\bar{c}$            mean aerodynamic chord (computed from wing planform area including theoretical apex area), in.
- $C_D$         drag coefficient,  $\frac{\text{Drag}}{qS}$
- $C_L$         lift coefficient,  $\frac{\text{Lift}}{qS}$

$\Delta C_L$	change in lift coefficient due to flap deflection, $(C_L)_{\delta_f} - (C_L)_{\delta_f=0}$
$C_m$	pitching-moment coefficient, $\frac{\text{Pitching moment}}{qS\bar{c}}$
$\Delta C_m$	change in pitching-moment coefficient due to flap deflection, $(C_m)_{\delta_f} - (C_m)_{\delta_f=0}$
$\frac{\partial C_m}{\partial C_N}$	static longitudinal stability parameter (longitudinal distance in percent of mean aerodynamic chord from center of gravity to aerodynamic-center location; positive forward, negative rearward)
$C_N$	normal-force coefficient, $\frac{\text{Normal force}}{qS}$
$C_n$	yawing-moment coefficient, $\frac{\text{Yawing moment}}{qSb}$
$C_Y$	side-force coefficient, $\frac{\text{Side force}}{qS}$
$L/D$	lift-drag ratio
$M$	free-stream Mach number
$q$	free-stream dynamic pressure, lb/sq in.
$S$	planform area of undeflected wing (including theoretical apex area and excluding flap area and aperture area), sq in.
$S_f$	flap (two) area, sq in.
$S_n$	planform area of deflected nose portion of wing (including theoretical apex area), sq in.
$S_{tf}$	tip-fin (two) area, sq in.
$\alpha$	angle of attack (referenced to bottom of undeflected wing), deg
$\beta$	angle of sideslip (referenced to wing root chord), deg





$\delta_f$  flap-deflection angle (positive when trailing edge is down, negative when trailing edge is up), deg

$\delta_n$  nose-deflection angle (positive when nose is up, negative when nose is down), deg

## APPARATUS AND MODELS

### Wind Tunnel, Balance, and Model Support


The investigation was conducted in the Langley 9-inch supersonic tunnel of the High Temperature Fluid Mechanics Section. This facility is a continuous, closed-return type of wind tunnel with provisions for controlling the humidity, temperature, and pressure of the enclosed air. During the tests the quantity of water vapor in the airstream was kept sufficiently low so that the effects of water condensation in the supersonic nozzle were negligible.

The balance system used was a six-component, external type which utilized mechanical, self-balancing beams for the force measurements. A detailed description of the balance is presented in the appendix of reference 8.

The models were sting mounted to the model support of the external balance system. In order to test the models over an angle-of-attack range up to  $90^\circ$ , three stings and two different mounting techniques were used. A straight sting mounted at the base of the model body was used to obtain angles of attack from  $-4^\circ$  to  $17^\circ$ . A  $50^\circ$  bent sting, a  $30^\circ$  bent sting, and a straight sting, mounted at the top of the body just ahead of the model base, were used to obtain angles of attack from  $17^\circ$  to  $36^\circ$ ,  $36^\circ$  to  $66^\circ$ , and  $66^\circ$  to  $90^\circ$ , respectively. Photographs of model C presented in figure 1 show the two sting-support locations on the model body. During the tests when the models were sting supported from the base of the model body the attachment protuberance on the top of the model body was removed and the hole was filled and contoured with the body. The stings were shielded from air loads by a movable windshield which was equipped with four pressure tubes open at the nose of the windshield to measure model base pressures. The streamwise gap between the model body and the nose of the windshield was maintained to within 0.03 inch for all tests.

### Models

The three models of this investigation were modified versions of model A of reference 1. These models had  $75^\circ$  sweptback delta wings with



hemicylindrically rounded leading edges. The wing tips were clipped to accommodate tip fins and the wing trailing edges were recessed to accommodate any one of seven sets of interchangeable flaps which produced flap deflections of  $0^\circ$ ,  $\pm 20^\circ$ ,  $\pm 50^\circ$ , and  $\pm 70^\circ$ . Apertures were located in the wing ahead of the flaps. The rear faces of the apertures were hemicylindrical. The purpose of the apertures was to increase the control effectiveness of negative flap deflections at positive angles of attack by producing a greater pressure on the leeward side of the flaps. These apertures also produce a positive shift in the slope of the pitching-moment curves by reducing the lifting surface of the wing rearward of the center-of-gravity location. Detailed drawings of the models are presented in figure 2 and some of the geometric properties of the models are presented in table I.

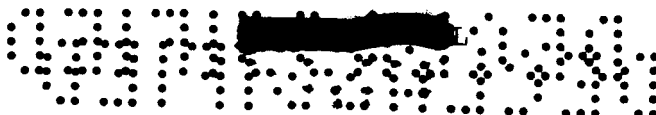
Model A of this investigation differed from model A used in reference 1 in that the wing panels in front of the apertures were beveled  $30^\circ$  as shown in figure 2(a). Models B and C had larger flaps than had model A and the leading edges of these flaps were located slightly ahead of the flap leading-edge location for model A. This decreased the aperture size for these models.

Models B and C had nose deflections of  $15^\circ$  and  $18^\circ$ , respectively, at a 54-percent-root-chord location. Small tip fins were mounted on models A and B at a roll-out angle of  $15^\circ$  and a toe-in angle of  $6.5^\circ$  for all tests. Model C had small tip fins mounted at a roll-out angle of  $30^\circ$  and a toe-in angle of  $10^\circ$  and large tip fins mounted at a roll-out angle of  $0^\circ$  and a toe-in angle of  $6.5^\circ$ . Both sets of tip fins were used on model C for the tests at a combined angle of attack and angle of sideslip and only the large tip fins were used on the model for the angle-of-attack tests.

## TESTS, MEASUREMENTS, AND CORRECTIONS

### Test Conditions and Procedure

All tests were made at a free-stream Mach number of 2.91. The test Reynolds numbers based on the mean aerodynamic chord of the models were  $0.68 \times 10^6$  for models A and C and  $1.28 \times 10^6$  for model B. The tests on models A and B were made over an angle-of-attack range from approximately  $36^\circ$  to  $60^\circ$  with flap deflections ranging from  $0^\circ$  to  $-50^\circ$ . The tests on model C were made over an angle-of-attack range from  $-4^\circ$  to  $90^\circ$  with flap deflections ranging from  $0^\circ$  to  $\pm 70^\circ$ . In addition, tests were made on model C over a combined angle-of-attack and angle-of-sideslip range with angles of attack up to  $51^\circ$ . The sideslip tests were made with the flaps undeflected.



## Measurements and Corrections

Lift, drag, pitching moment, side force, and yawing moment were measured on an external balance system. The angle of attack and angle of sideslip of the models were determined with an optical system for indicating pitch and yaw attitude. In this system small (1/16-inch-diameter) mirrors were attached to the models on the bottom of the wing or on the tip fins. These mirrors reflected an image from an external light source onto a graduated scale. With this method the true angle was obtained irrespective of the model deflection under load. Standard corrections for sting-mounted models in the Langley 9-inch supersonic tunnel were applied to the drag data of the models to correct the base pressure inside the windshield to free-stream static-pressure conditions.

The discontinuity found in the lift, pitching-moment, and drag data of model C is due primarily to sting-windshield interference effects. These interference effects which varied with the different sting-mounting techniques are most pronounced over the angle-of-attack range starting at  $\alpha = 17^\circ$ . At this angle the sting was mounted in the top of the body and the windshield was not completely shadowed by the wing from the air-stream. However, as the angle of attack was increased, the interference effects were reduced.

The probable errors due solely to stream calibration inaccuracies are estimated to be within  $\pm 0.01$  for Mach number and  $\pm 0.05$  for angles of attack and sideslip.

## RESULTS AND DISCUSSION

### Model A of Reference 1 and Present Model A

The longitudinal aerodynamic characteristics of model A of reference 1 and model A of this investigation are presented in figure 3. Model A differed from model A of reference 1 in only one respect. The wing sections in front of the apertures were beveled  $30^\circ$  as shown in figure 2(a). The purpose of the bevel was to increase the control effectiveness of negative flap deflections at positive angles of attack by increasing the aperture area through which the air could pass, thus increasing the pressure on the leeward side of the flaps. The pitching-moment data presented in figure 3(a) for model A of reference 1 are given about a center-of-gravity location at 58 percent of the body length in order to compare directly these data with the data from the models of this investigation. Figure 3(a) shows that model A of reference 1 with flap deflections of  $0^\circ$ ,  $-20^\circ$ , and  $-50^\circ$  is longitudinally stable over the angle-of-attack range presented. The results of

figure 3(b) indicate that model A of the present investigation with flap deflections of  $0^\circ$ ,  $-20^\circ$ , and  $-50^\circ$  is longitudinally unstable from approximately  $\alpha = 40^\circ$  to  $\alpha = 52^\circ$  and longitudinally stable from approximately  $\alpha = 52^\circ$  to  $\alpha = 60^\circ$ .

#### Model B

Figure 4 presents the longitudinal aerodynamic characteristics of model B. Results show that model B is longitudinally stable with flap deflections of  $0^\circ$  and  $-50^\circ$  over the complete angle-of-attack range of the tests. A slight extrapolation of the data shows that model B can be trimmed and is stable at an angle of attack near  $38^\circ$  with a flap deflection of  $-50^\circ$ .

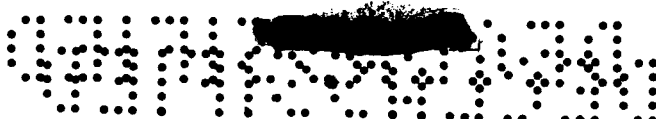
#### Model C

Basic data.— The longitudinal aerodynamic characteristics of model C with large, vertical tip fins are presented in figure 5. The angle-of-attack range for each of the four model mounting techniques is also indicated in this figure. The results indicate, in general, that model C is longitudinally stable through the complete angle-of-attack range up to  $90^\circ$  for zero and negative flap deflections. However, for positive flap deflections the angle-of-attack range for which the model was stable decreased for increasing deflection angle. The angle of attack for maximum lift varied from about  $38^\circ$  for a flap deflection of  $50^\circ$  to about  $46^\circ$  for a flap deflection of  $-70^\circ$ . The maximum lift-drag ratio varied from about 1.1 to 1.9 depending on the flap-deflection angle.

In figure 6 the curves for  $C_m$  and  $C_L$  of model C for various flap deflections are presented over the angle-of-attack range near maximum lift. The results show that model C is longitudinally stable up to the maximum lift range for all flap deflections.

Control effectiveness.— Figure 7 presents the incremental change in  $C_L$  and  $C_m$  due to flap deflection for model C with large, vertical tip fins. For negative flap deflections ( $\delta_f = -20^\circ$  to  $-70^\circ$ ) the results indicate, in general, an increase of control effectiveness with angle of attack. Considering positive flap deflections (above  $\delta_f = 20^\circ$ ) in the higher angle-of-attack range (above  $\alpha = 45^\circ$ ), the results indicate a decrease in control effectiveness.

Longitudinal trim characteristics.— In figure 8 the longitudinal trim characteristics are presented for model C with large, vertical tip fins. The results indicate that model C can be trimmed longitudinally



and is stable over an angle-of-attack range from  $-4^\circ$  to  $41^\circ$ . The trim-lift-coefficient values ranged from 0.13 at an angle of attack of  $-4^\circ$  with a flap deflection of  $50^\circ$  to 0.63 at an angle of attack of  $41^\circ$  with flap deflections of  $-50^\circ$  and  $-70^\circ$ .

Comparison with theory.- There is no available supersonic theory to predict the forces on a model having a detached shock at a Mach number of 2.91. However, a comparison is made in figure 9 of the experimental values of  $C_L$  and  $C_D$  of model C with two estimates obtained by using hypersonic theories. One estimate was obtained from a semi-empirical method of prediction presented in reference 2. The other estimate was obtained from modified Newtonian theory, in which wing-thickness effects were ignored. The results of the comparison made in figure 9 indicate that both theoretical estimates predict the angle of attack for zero lift and the angle of attack for maximum lift. At angles of attack above maximum lift (above  $\alpha = 46^\circ$ ) the theoretical estimates of lift from modified Newtonian theory more closely agree with experimental results; in the low angle-of-attack range ( $\alpha = 0^\circ$  to  $25^\circ$ ), however, the estimates obtained by use of the method of reference 2 are in closer agreement with experimental results. In general, however, neither theory is particularly successful in the intermediate angle-of-attack range ( $\alpha = 25^\circ$  to  $50^\circ$ ). This might be expected since both theories would be more properly applied to results at Mach numbers higher than 2.91. The experimental drag results shown in figure 9 also are in closer agreement with theoretical results obtained by use of the method of reference 2 in the lower angle-of-attack range and with those obtained from modified Newtonian theory near an angle of attack of  $90^\circ$ .

Directional stability characteristics.- The directional stability characteristics of model C are presented in figure 10. The results indicate that model C is directionally stable with large, vertical tip fins at angles of attack of  $0^\circ$ ,  $30^\circ$ , and  $50^\circ$ . With small, rolled-out tip fins the results show that model C is directionally stable at angles of attack of  $30^\circ$  and  $50^\circ$ . It is interesting to note that the small tip fins produce greater directional stability than do the large tip fins at an angle of attack of  $30^\circ$ . However, it should be remembered that these small fins were not only toed-in  $10^\circ$  but also rolled-out  $30^\circ$ , whereas the large fins were only toed-in  $6.5^\circ$  and had no roll-out.

#### Comparison of Models

Effects of modifications.- A comparison of the incremental change in  $C_m$  and  $C_L$  due to negative flap deflection over the angle-of-attack range near maximum lift is presented in figure 11 for model A of reference 1, and models A, B, and C with large, vertical tip fins. In general this figure shows the effects of beveling the wing in front



of the apertures, nose deflection, flap size, and tip-fin size on the incremental lift and control effectiveness. Comparing the results of model A of reference 1 and model A of the present tests indicates that the bevel produced a small increase in control effectiveness and a small reduction in incremental lift for negative flap deflections. A comparison of the results of models B and C indicates that an increased nose deflection from  $15^\circ$  to  $18^\circ$  and a change in tip fins from small to large produced approximately the same effect on control effectiveness and incremental lift as did the bevel. A comparison of the results of model A of reference 1 and model B indicates that a nose deflection of  $15^\circ$  and the use of larger flaps more than doubled the control effectiveness and the loss in incremental lift for negative flap deflections.

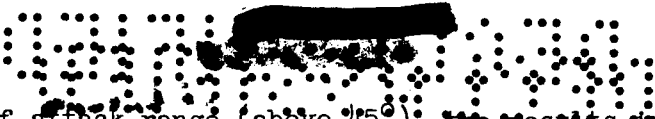
Longitudinal stability characteristics.— Figure 12 presents a comparison of the lift coefficients and longitudinal stability parameters  $\partial C_m / \partial C_N$  for model A of reference 1, and models A, B, and C with large, vertical tip fins. The data are presented for the angle-of-attack range near maximum lift and for flap deflections of  $0^\circ$ ,  $-20^\circ$ , and  $-50^\circ$ . The results show that models B and C are longitudinally stable over the maximum lift range. Model A of reference 1 is longitudinally stable with flap deflections of  $0^\circ$  and  $-50^\circ$  but becomes unstable at an angle of attack of  $54^\circ$  with a flap deflection of  $-20^\circ$ . Model A is longitudinally unstable to approximately the angle of attack of maximum lift for each flap deflection and stable over the remainder of the angle-of-attack range.

## CONCLUSIONS

An investigation was made at a Mach number of 2.91 to determine the stability and control characteristics of three lifting reentry configurations. The results of the investigation indicate the following conclusions:

1. The model with a nose deflection of  $18^\circ$  and large, vertical tip fins could be trimmed longitudinally and was stable over an angle-of-attack range from  $-4^\circ$  to  $41^\circ$ . The trim lift-coefficient values ranged from 0.13 at an angle of attack of  $-4^\circ$  with a flap deflection of  $50^\circ$  to 0.63 at an angle of attack of  $41^\circ$  with flap deflections of  $-50^\circ$  and  $-70^\circ$ . At test angles of attack this model with both large, vertical tip fins and small, rolled-out tip fins was directionally stable.

2. For negative flap deflections ( $-20^\circ$  through  $-70^\circ$ ), the results indicate, in general, an increase of control effectiveness with angle of attack. Considering positive flap deflections (above  $20^\circ$ ) in the

  
higher angle-of-attack range (above  $45^\circ$ ); the results indicate a decrease in control effectiveness.

3. Beveling the wing in front of the apertures produced a small increase in control effectiveness and a small reduction in incremental lift for negative flap deflections.

Langley Research Center,  
National Aeronautics and Space Administration,  
Langley Field, Va., November 16, 1960.

L  
1  
0  
0  
2

## REFERENCES

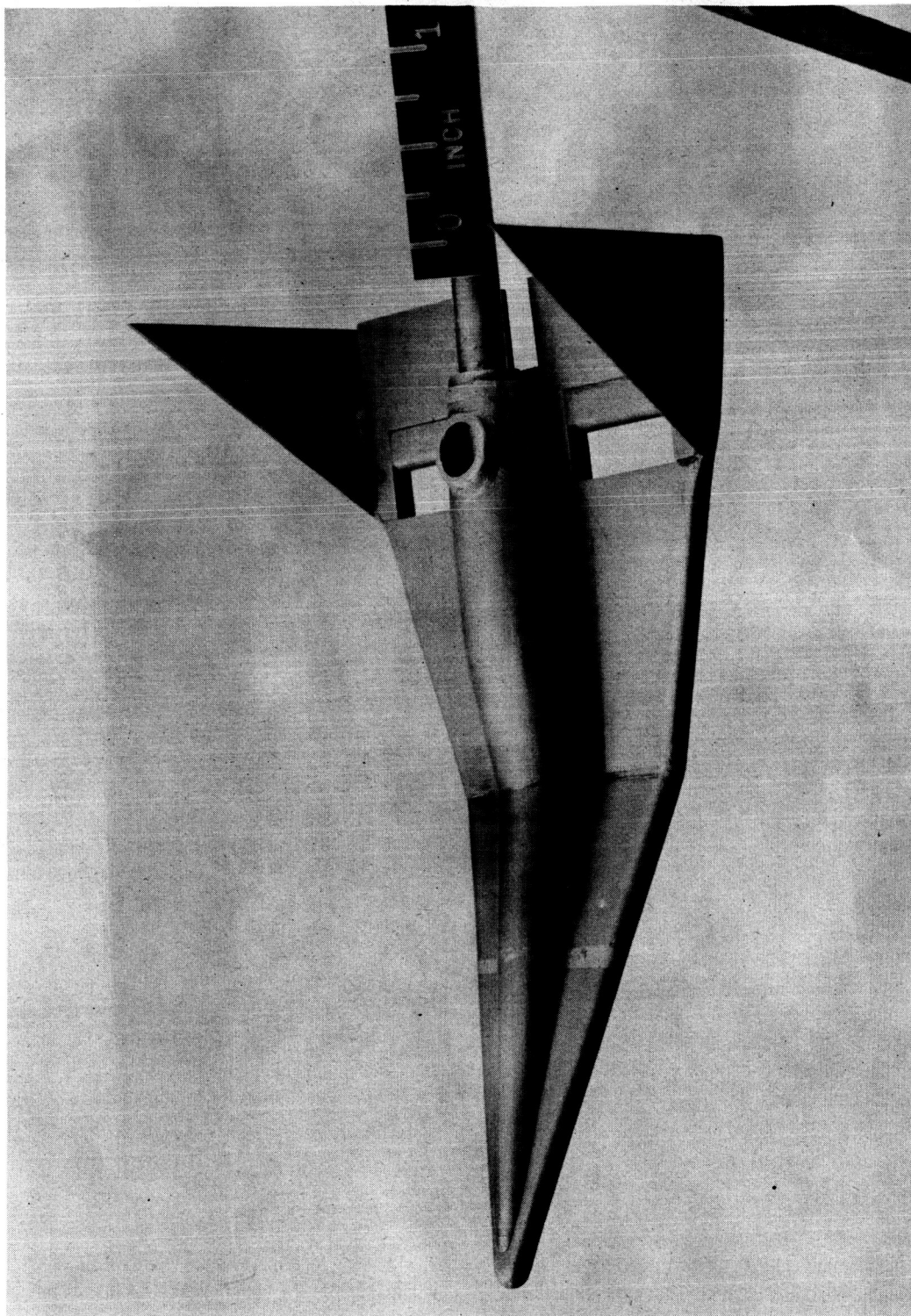
1. Clark, Frank L., and Evans, Joanna M.: Some Aerodynamic and Control Studies of Lifting Reentry Configurations at Angles of Attack up to  $90^\circ$  at a Mach Number of 2.91. NASA TM X-338, 1960.
2. Close, William H.: Hypersonic Longitudinal Trim, Stability, and Control Characteristics of a Delta-Wing Configuration at High Angles of Attack. NASA TM X-240, 1960.
3. Rainey, Robert W., and Close, William H.: Studies of Stability and Control of Winged Reentry Configurations. NASA TM X-327, 1960.
4. Paulson, John W.: Low-Speed Static Stability Characteristics of Two Configurations Suitable for Lifting Reentry From Satellite Orbit. NASA MEMO 10-22-58L, 1958.
5. Spencer, Bernard, Jr.: High-Subsonic-Speed Investigation of the Static Longitudinal Aerodynamic Characteristics of Several Delta-Wing Configurations for Angles of Attack From  $0^\circ$  to  $90^\circ$ . NASA TM X-168, 1959.
6. Foster, Gerald V.: Exploratory Investigation at Mach Number of 2.01 of the Longitudinal Stability and Control Characteristics of a Winged Reentry Configuration. NASA TM X-178, 1959.
7. Fournier, Paul G.: Wind-Tunnel Investigation at High Subsonic Speed of the Static Longitudinal Stability Characteristics of a Winged Reentry Vehicle Having a Large Negatively Deflected Flap-Type Control Surface. NASA TM X-179, 1959.
8. Rainey, Robert W.: Investigation of the Effects of Bomb-Bay Configuration Upon the Aerodynamic Characteristics of a Body With Circular Cross Section at Supersonic Speeds. NACA RM L55E27, 1955.



TABLE I.- GEOMETRIC CHARACTERISTICS OF MODELS

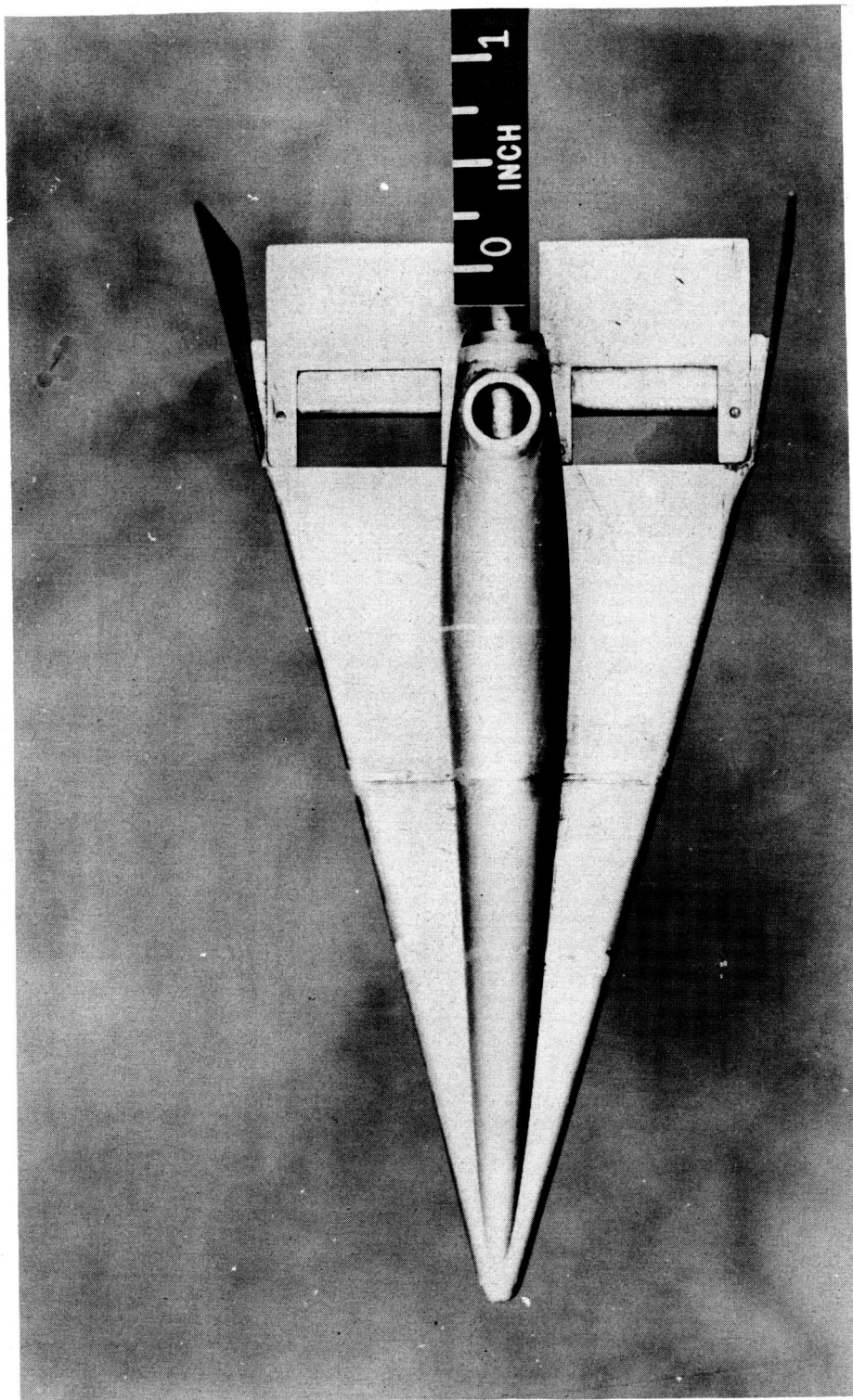
	Model A	Model B	Model C
Mean aerodynamic chord, $\bar{c}$ , in. . . . .	3.271	3.271	3.271
Wing span, b, in. . . . .	2.46	2.46	2.46
Planform area of undeflected wing, S, sq. in. . . . .	5.875	5.875	5.875
Ratio of deflected nose area to undeflected wing area, $S_n/S$ . . . . .	-----	0.36	0.36
Ratio of flap area to undeflected wing area, $S_f/S$ . . . . .	0.072	0.208	0.208
Ratio of tip-fin area to undeflected wing area, $S_{tf}/S$ . . . . .	0.162	0.162	0.162 and 0.338
Nose hinge-line location, percent c . . . . .	-----	54	54
Nose-deflection angle, $\delta_n$ , deg . . . . .	0	15	18

SECRET



(a) Three-quarter top view. L-59-7132

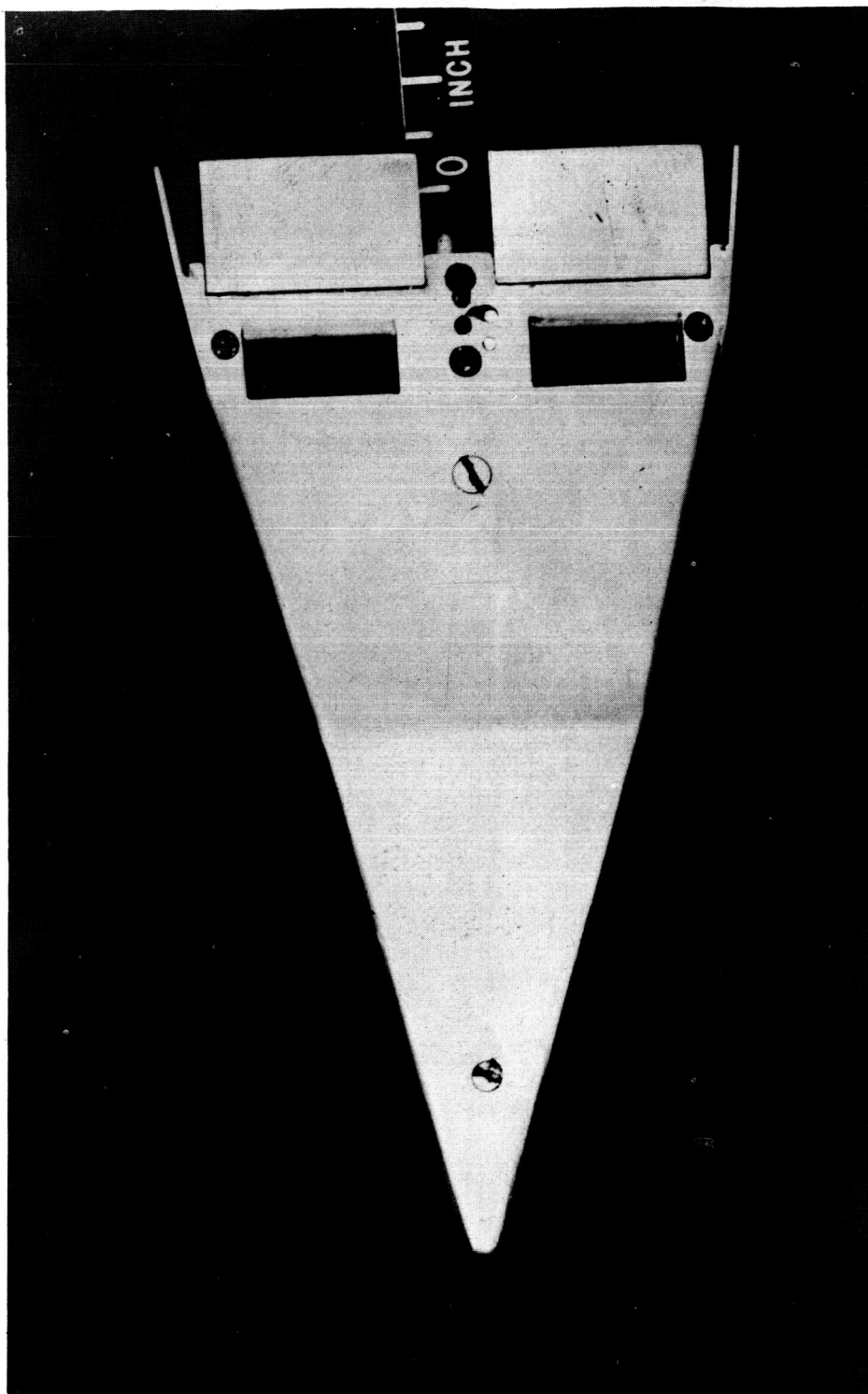
Figure 1.- Model C used in the present study.



(b) Top view. L-59-7133

Figure 1.- Continued.

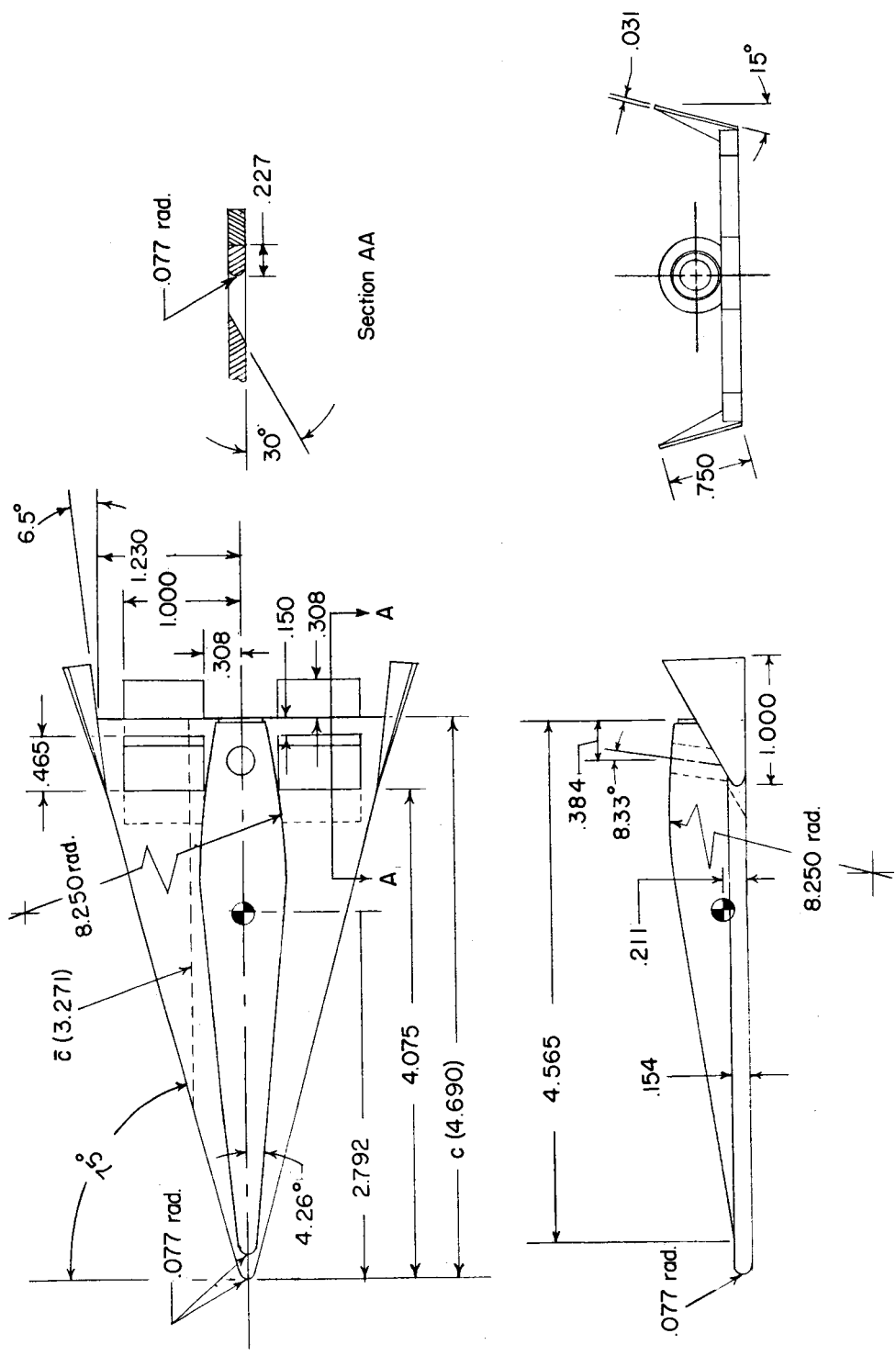
SECRET



(c) Bottom view. L-59-7134

Figure 1.- Concluded.

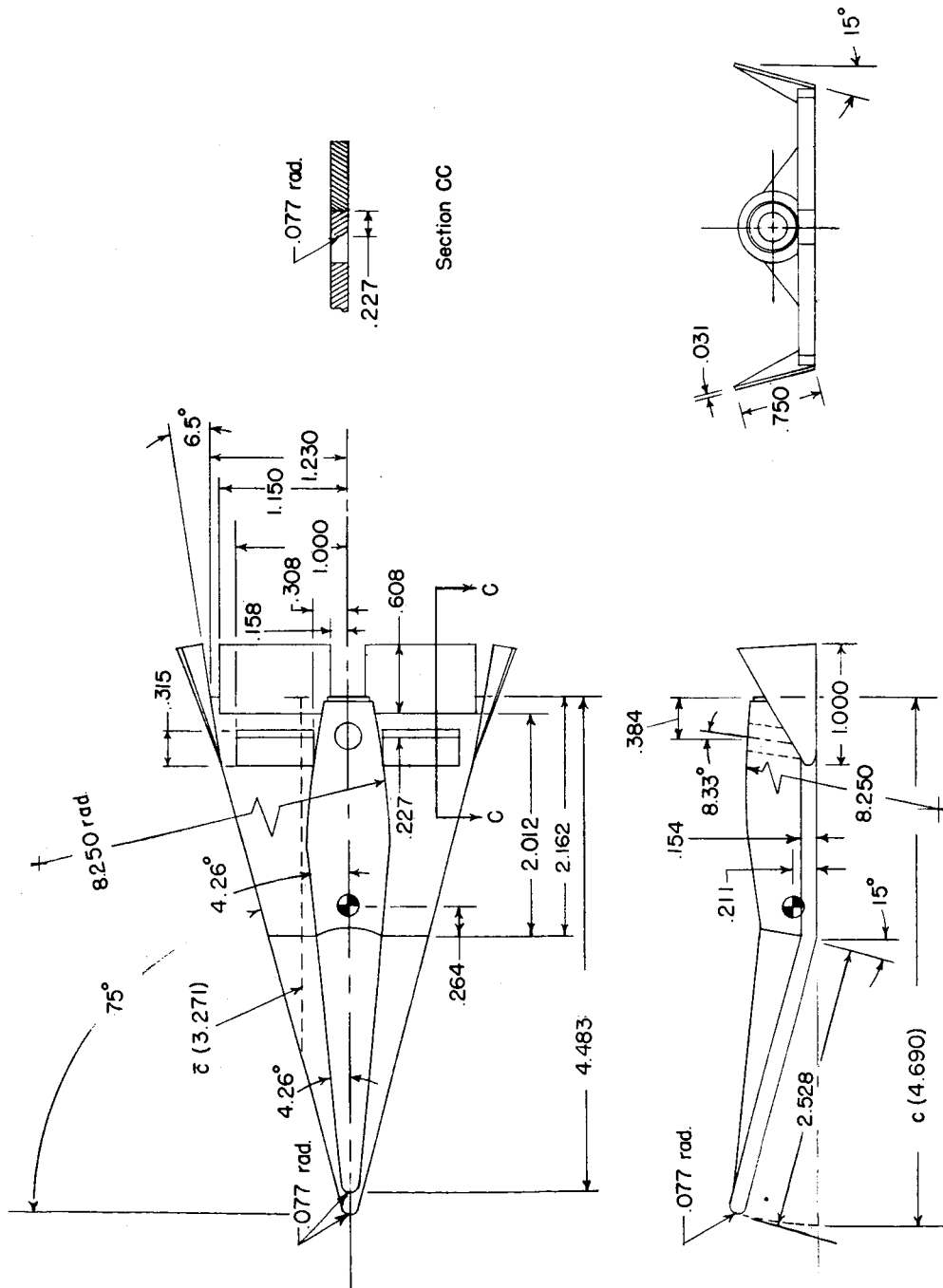
CONFIDENTIAL



(a) Model A.

Figure 2.- Detailed dimensions of models. (All dimensions are in inches unless otherwise indicated.)

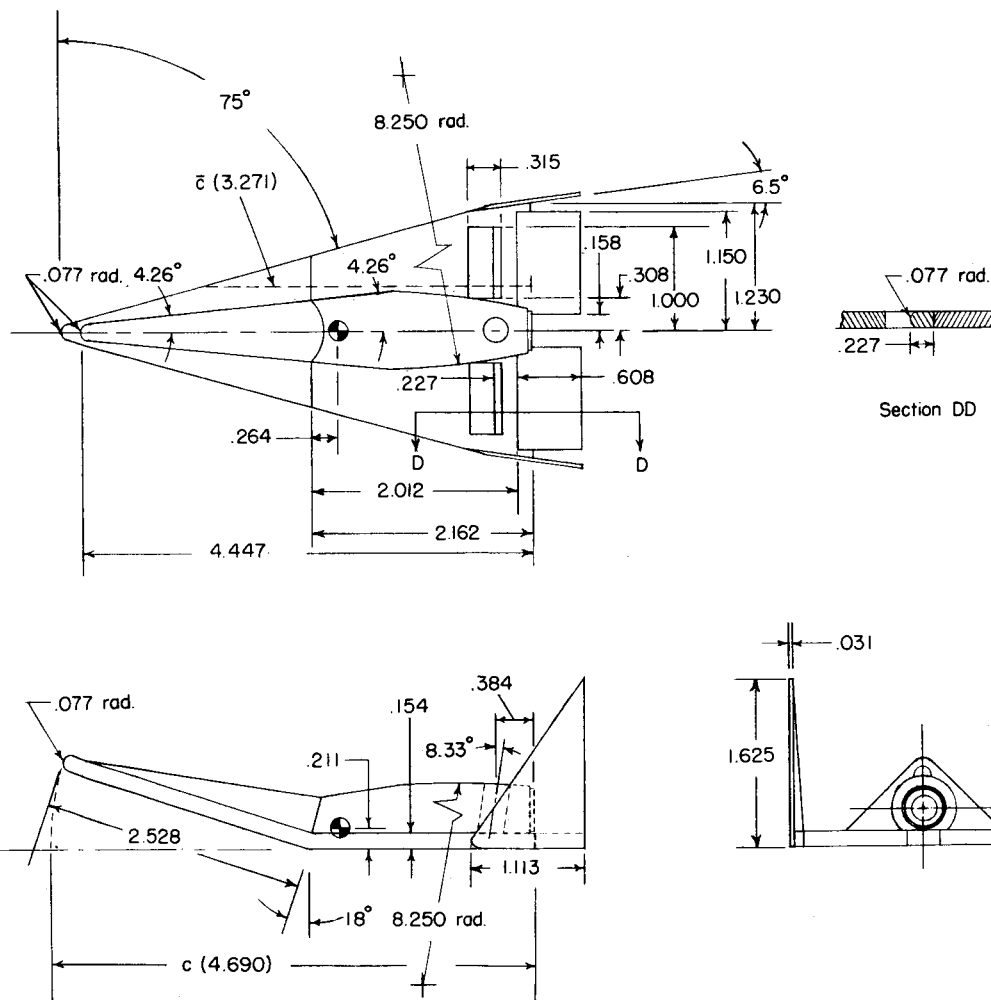
SECRET



(b) Model B.

Figure 2.- Continued.

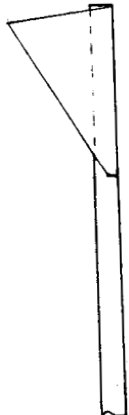
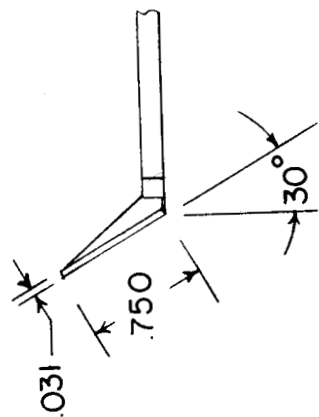
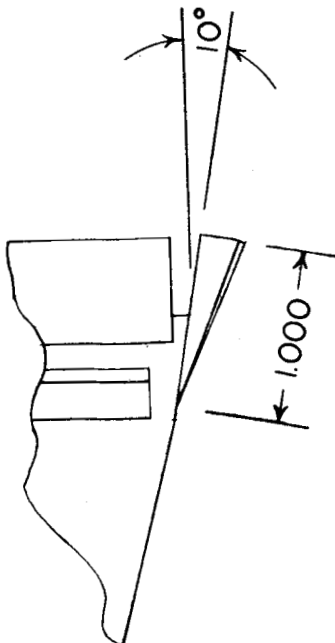
0371 [REDACTED] 00



(c) Model C with large tip fins.

Figure 2.- Continued.

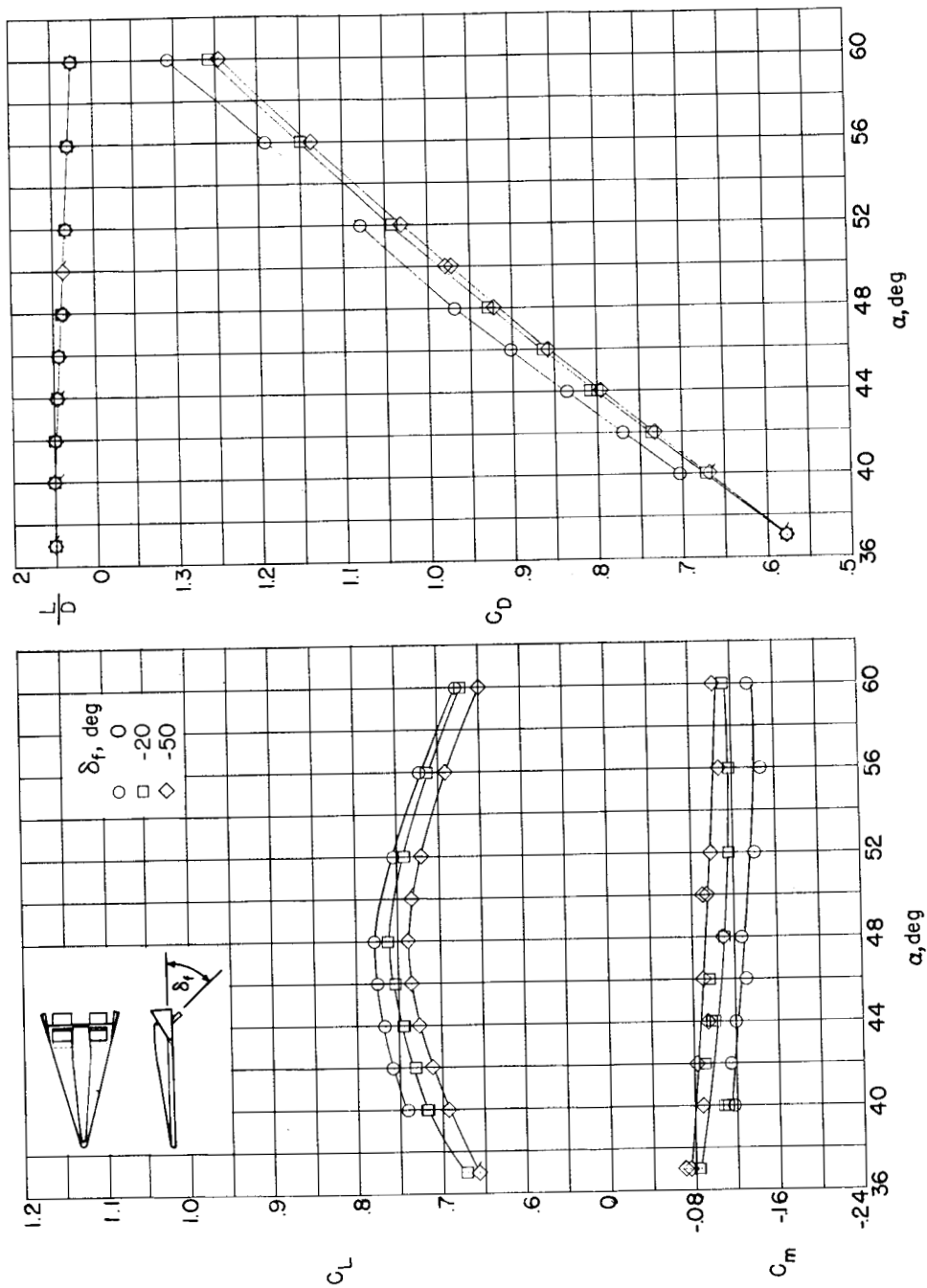
RECEIVED



(d) Model C with small tip fins.

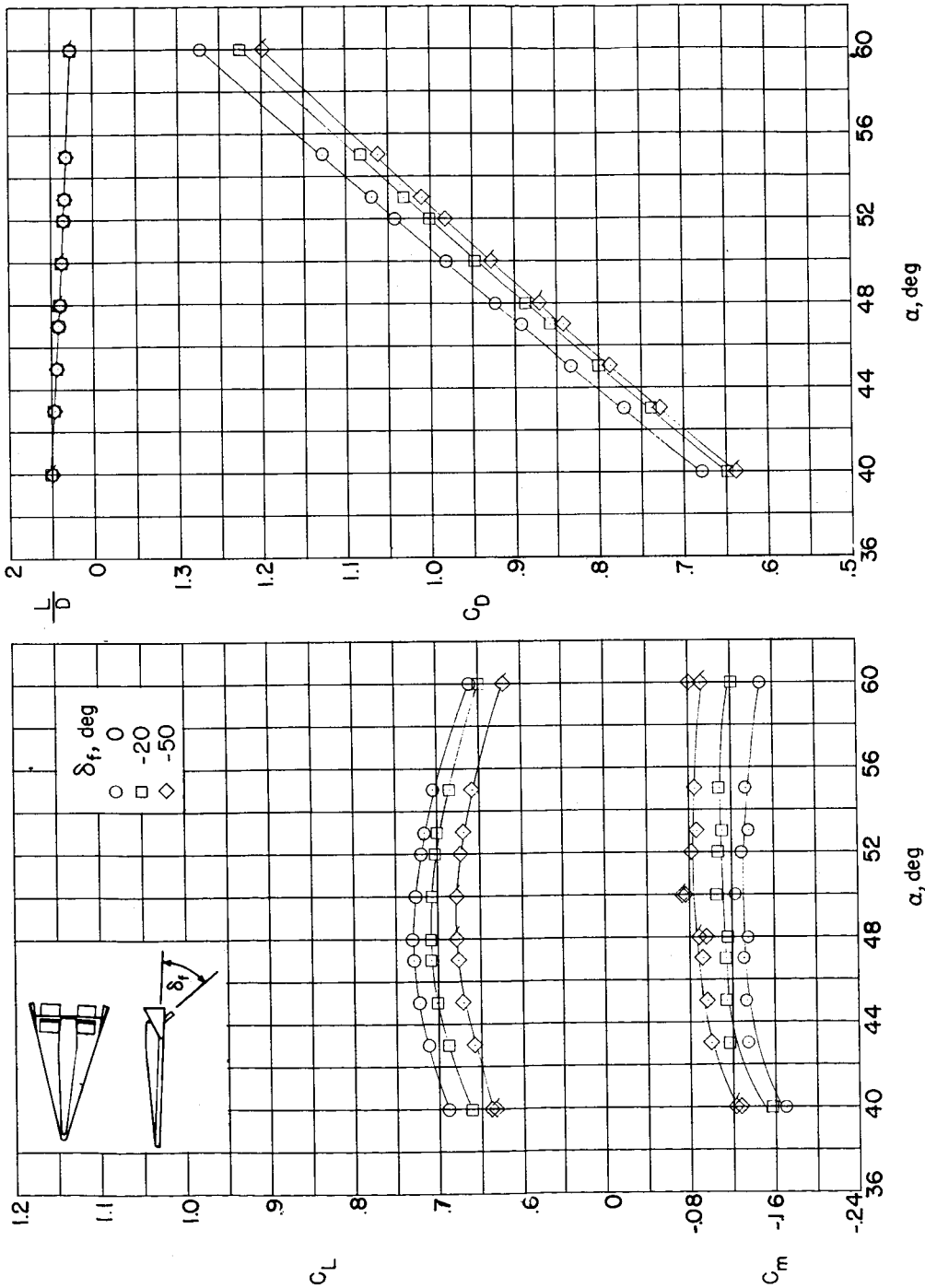
Figure 2.- Concluded.





(a) Model A of reference 1. (Flagged symbols denote check points.)

Figure 3.- Longitudinal aerodynamic characteristics of model A of reference 1 and model A of present investigation.



(b) Model A of present investigation. (Flagged symbols denote check points.)

Figure 3.- Concluded.

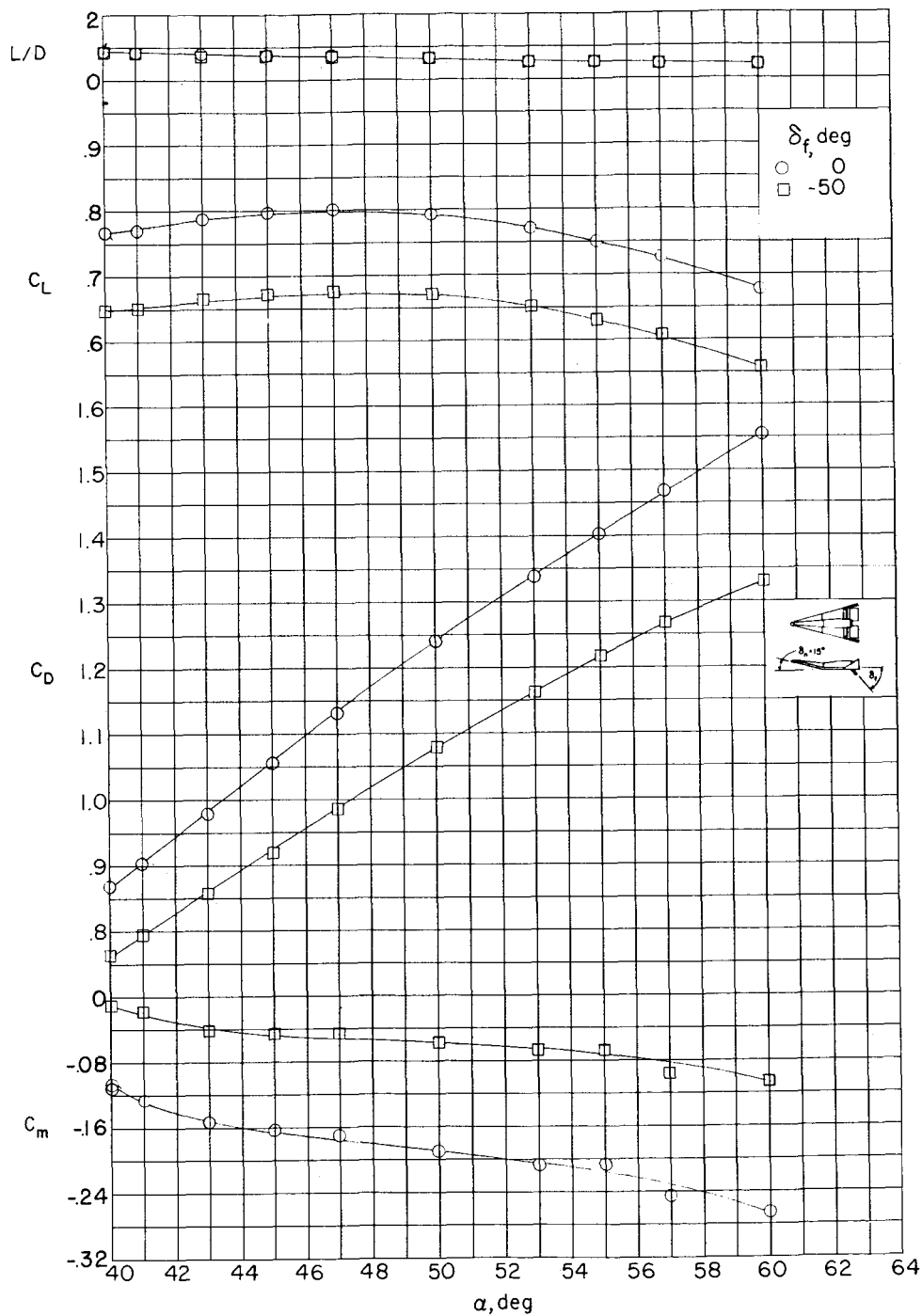


Figure 4.- Longitudinal aerodynamic characteristics of model B.  
 (Flagged symbols denote check points.)

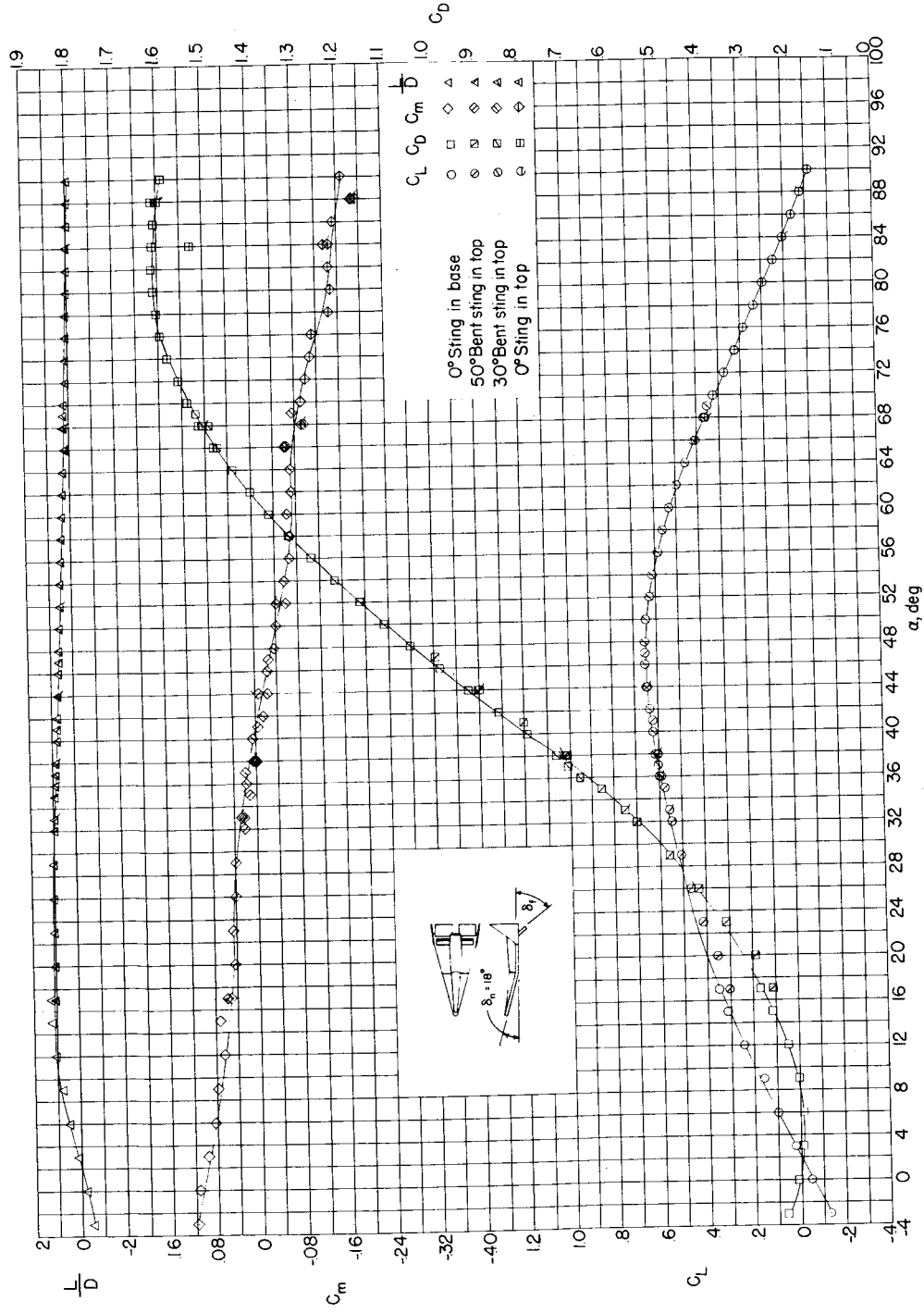
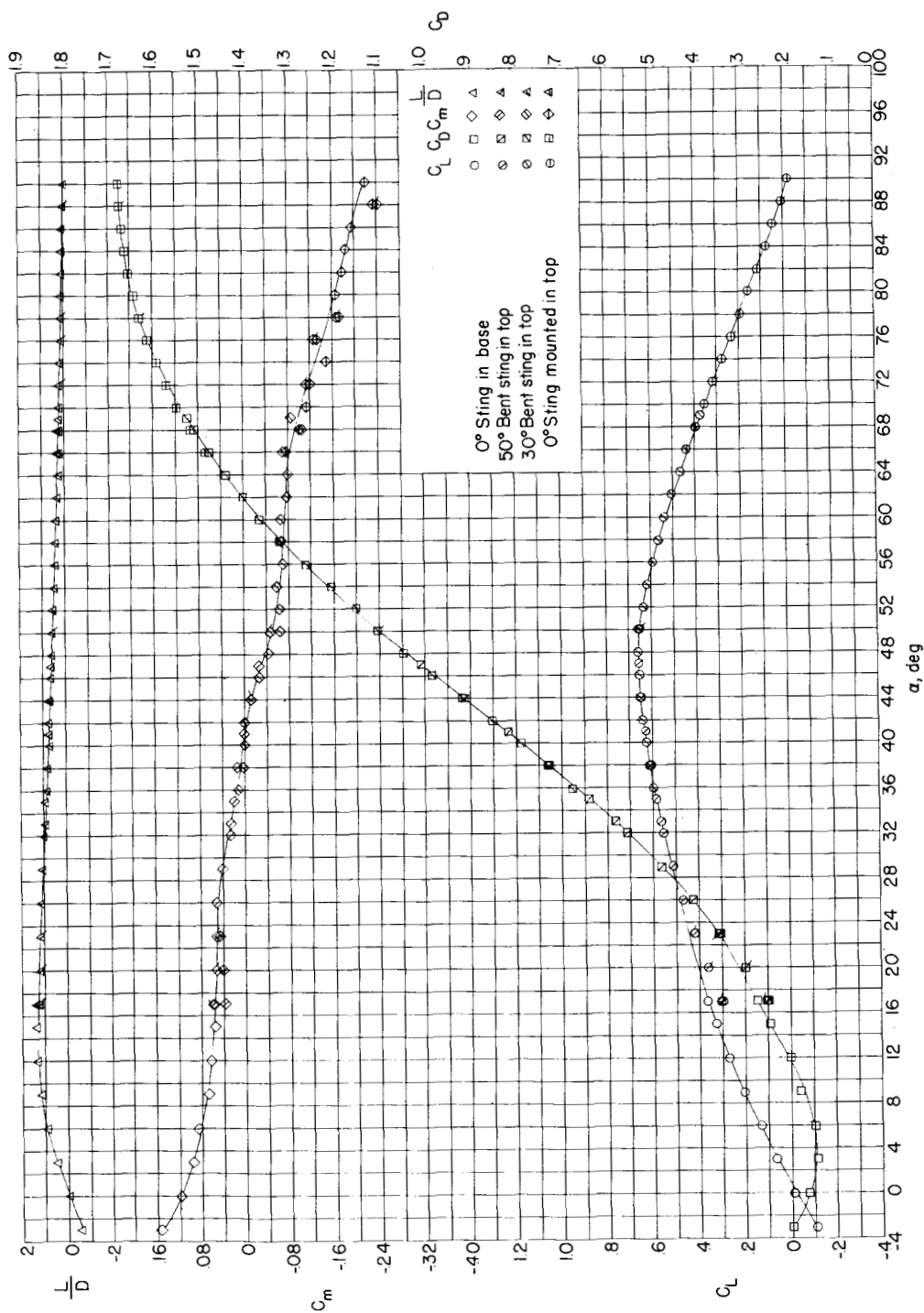
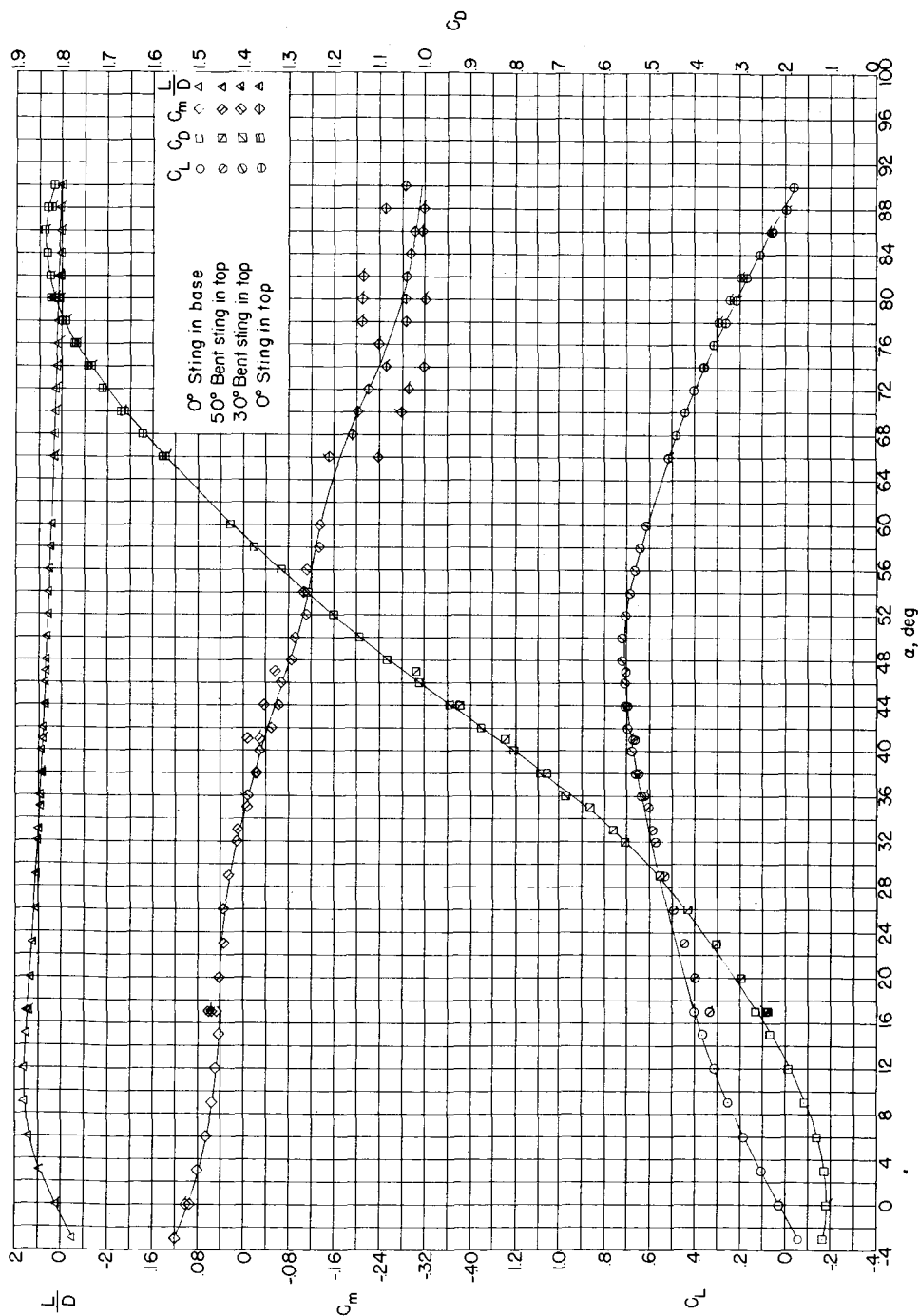
(a)  $\delta_f = -70^\circ$ .

Figure 5.- Longitudinal aerodynamic characteristics for model C with large tip fins. (Flagged symbols denote check points.)



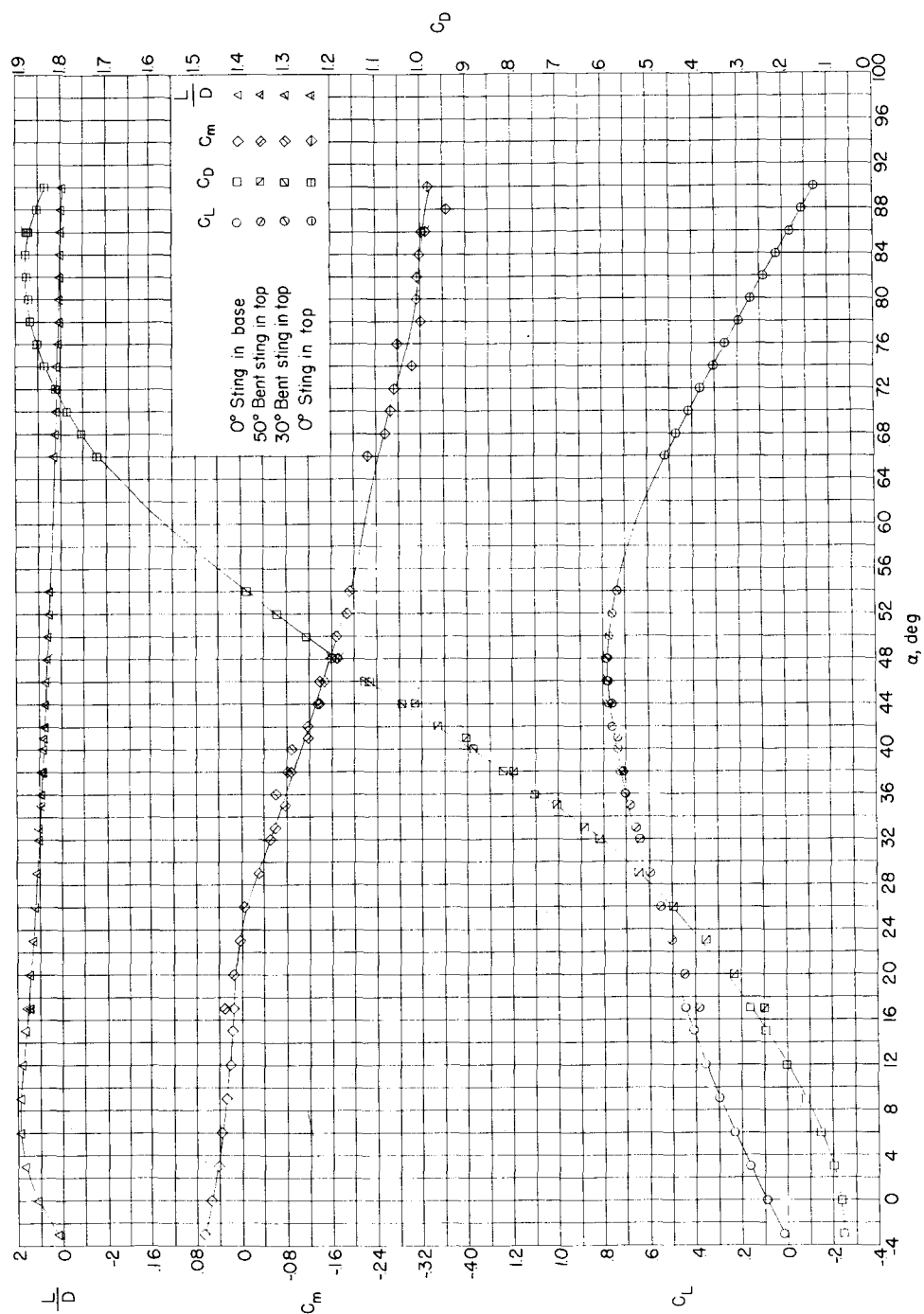
(b)  $\delta_f = -50^\circ$ .

Figure 5.- Continued.



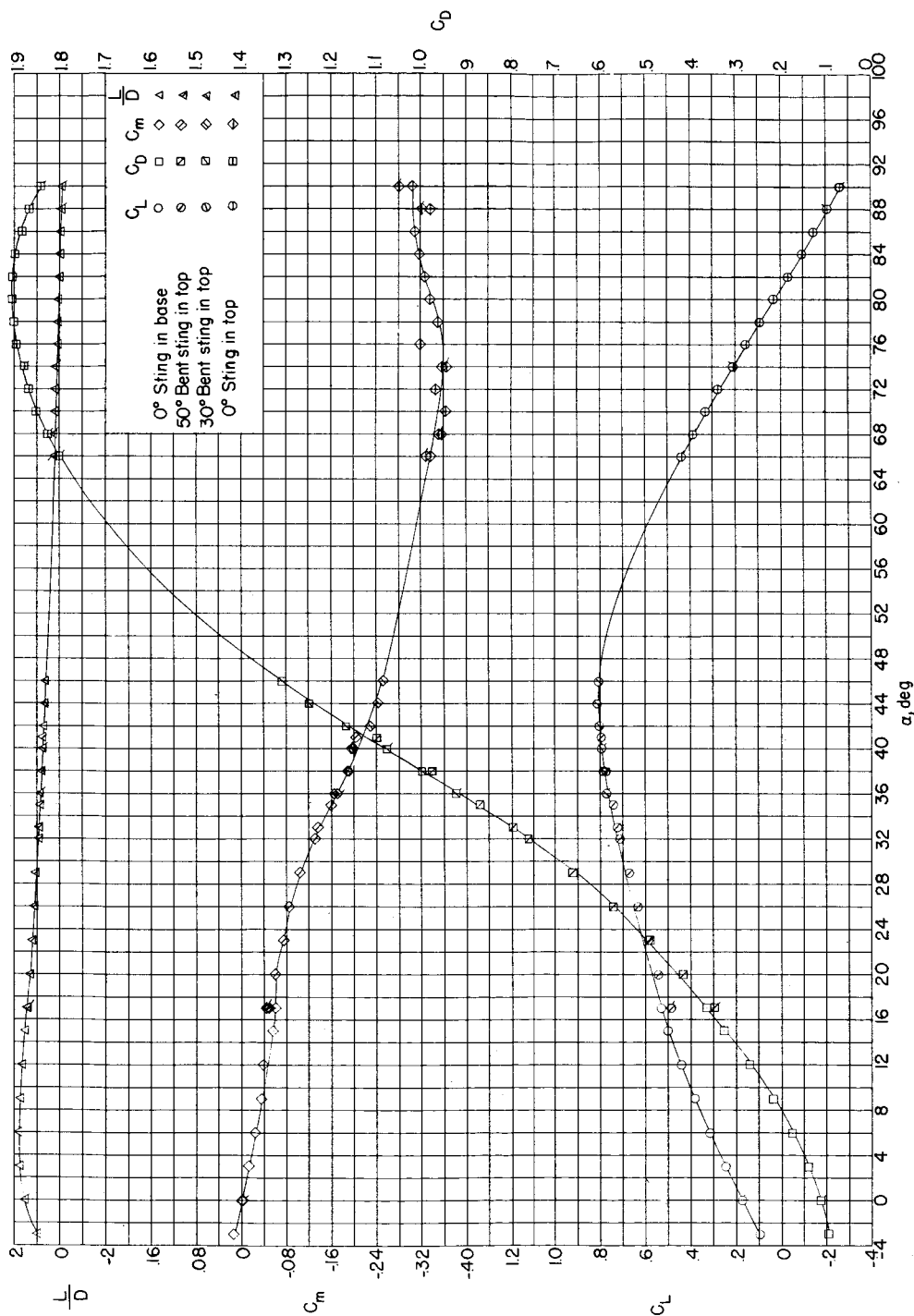
(c)  $\delta_f = -20^\circ$ .

Figure 5.- Continued.



(d)  $\delta_f = 0^\circ$ .

Figure 5.- Continued.

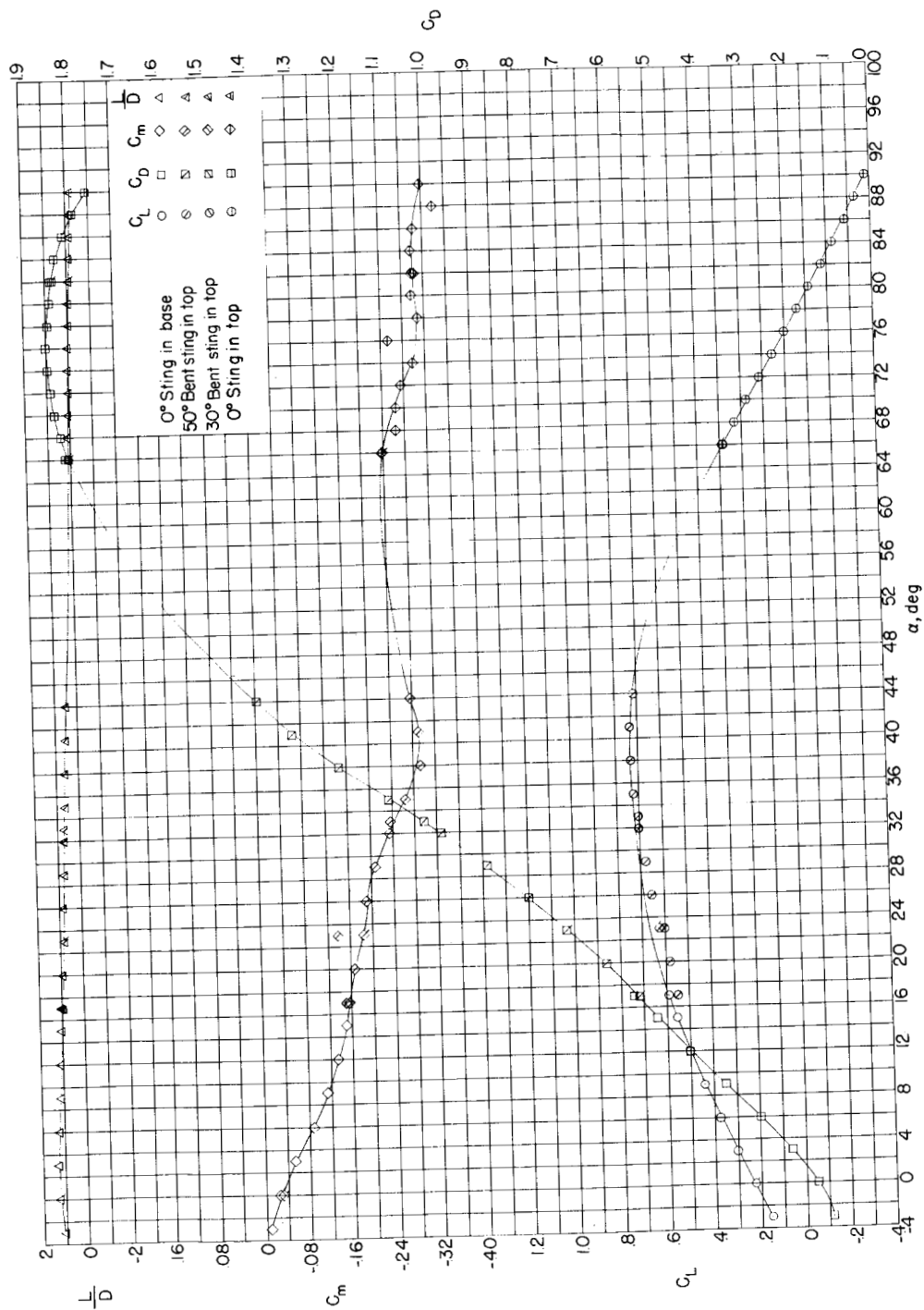


(e)  $\delta_f = 20^\circ$ .

Figure 5.- Continued.



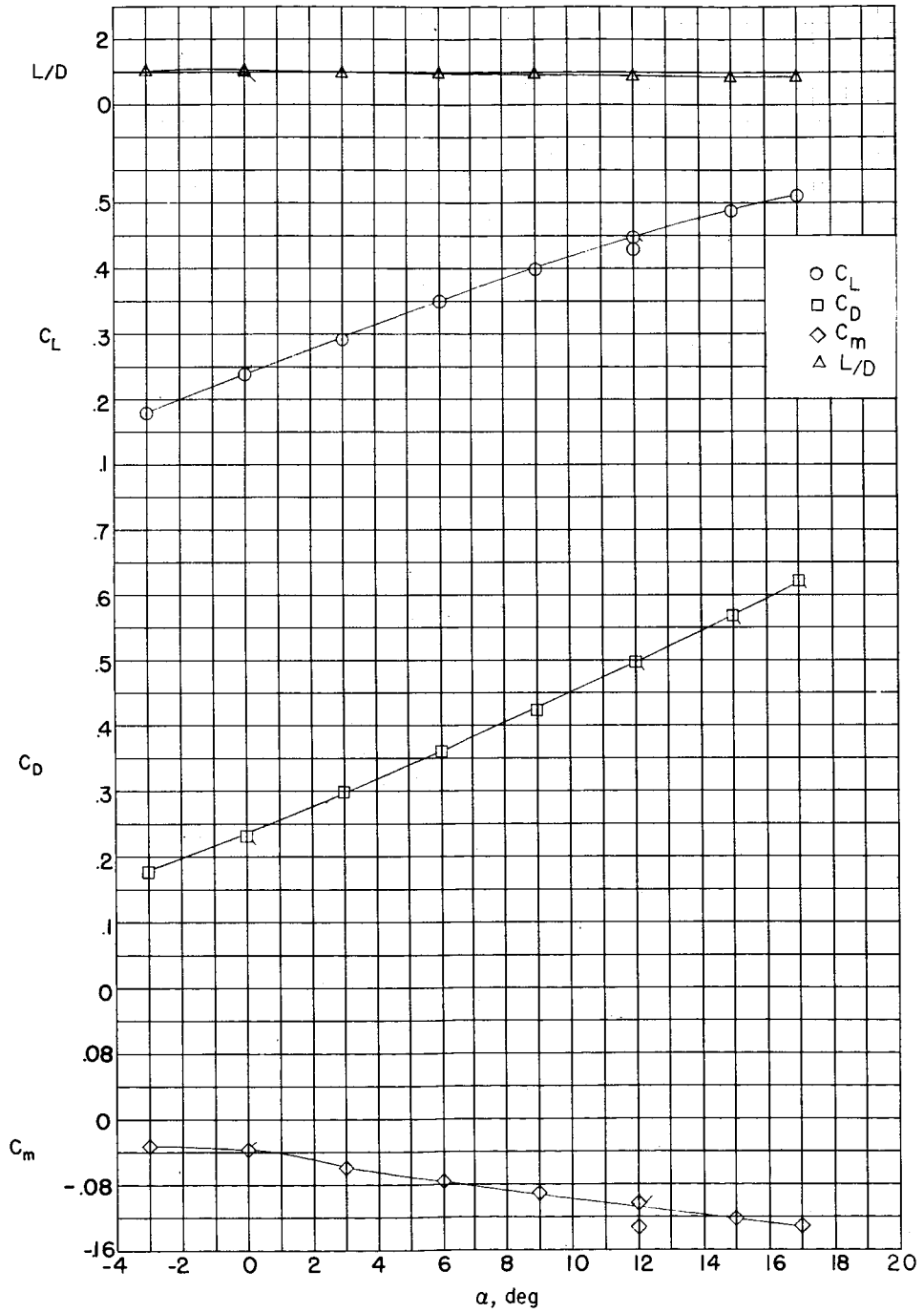
CONFIDENTIAL



(f)  $\delta_f = 50^\circ$ .

Figure 5.- Continued.

SECRET



(g)  $\delta_f = 70^\circ$ .

Figure 5.- Concluded.

SECRET

03: [REDACTED] 030

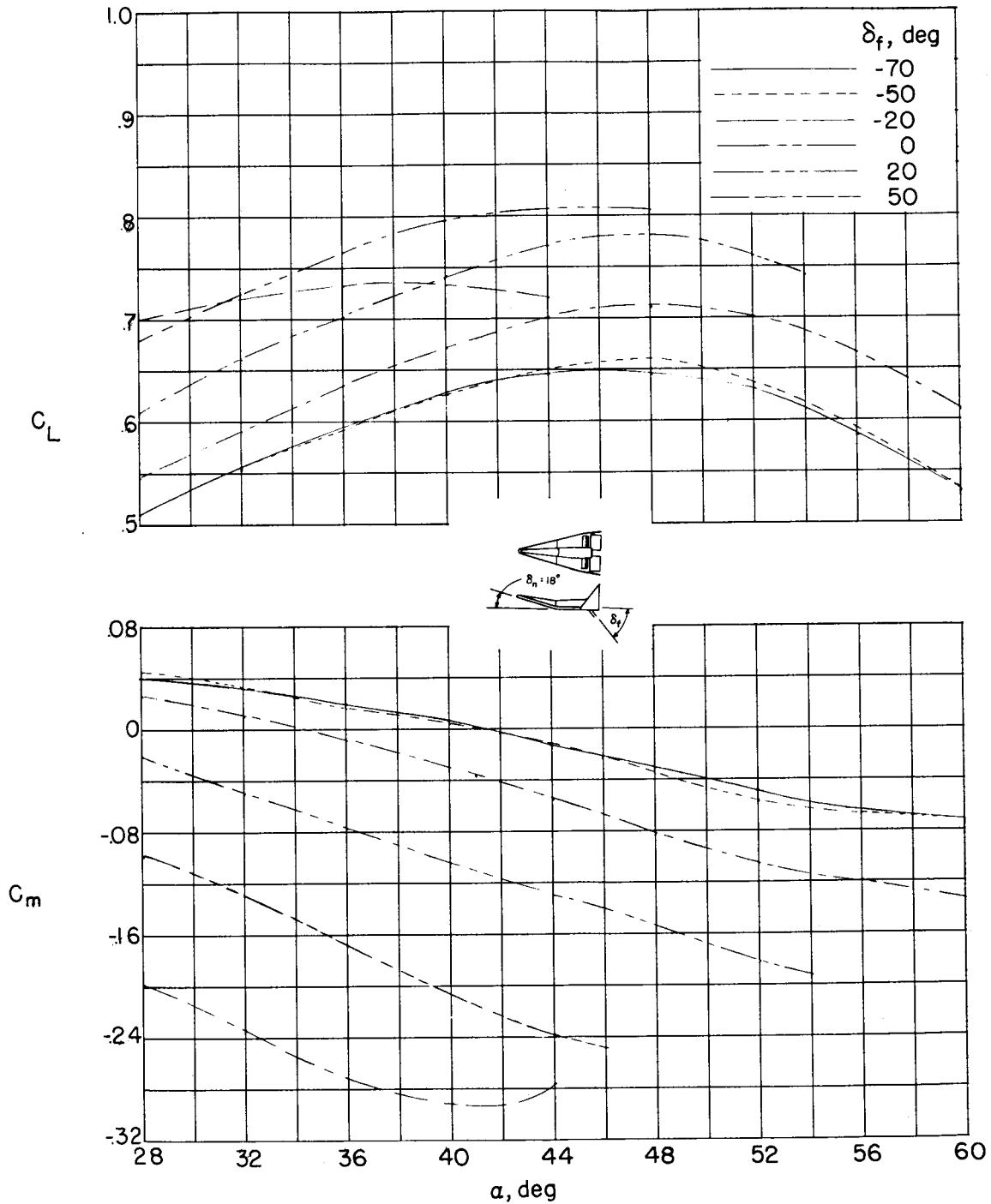


Figure 6.- Effect of flap deflection on  $C_L$  and  $C_m$  for model C with large tip fins.

[REDACTED]

CONFIDENTIAL

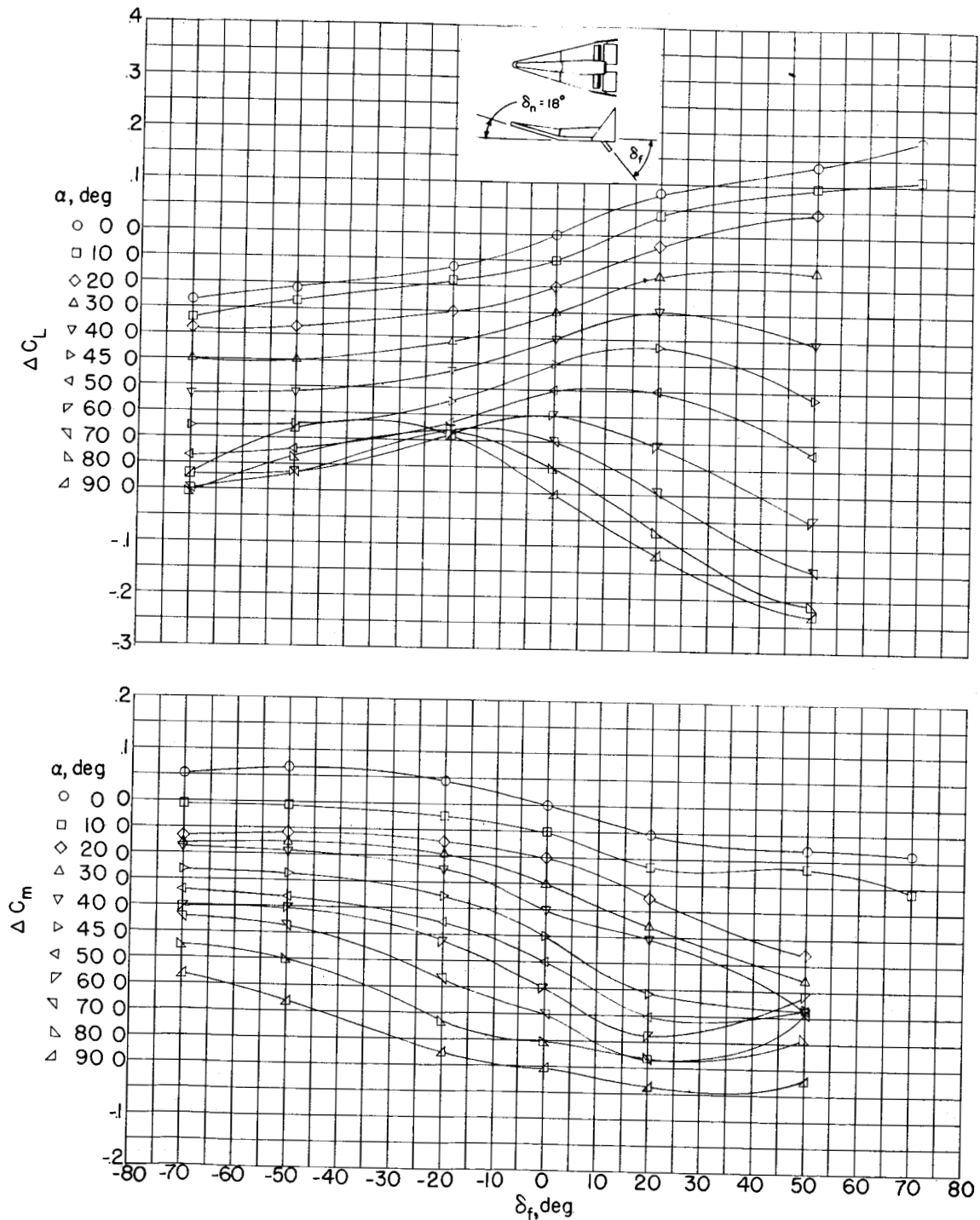


Figure 7.- Incremental change in  $C_L$  and  $C_m$  due to flap deflection for model C with large tip fins.

CONFIDENTIAL



DECLASSIFIED

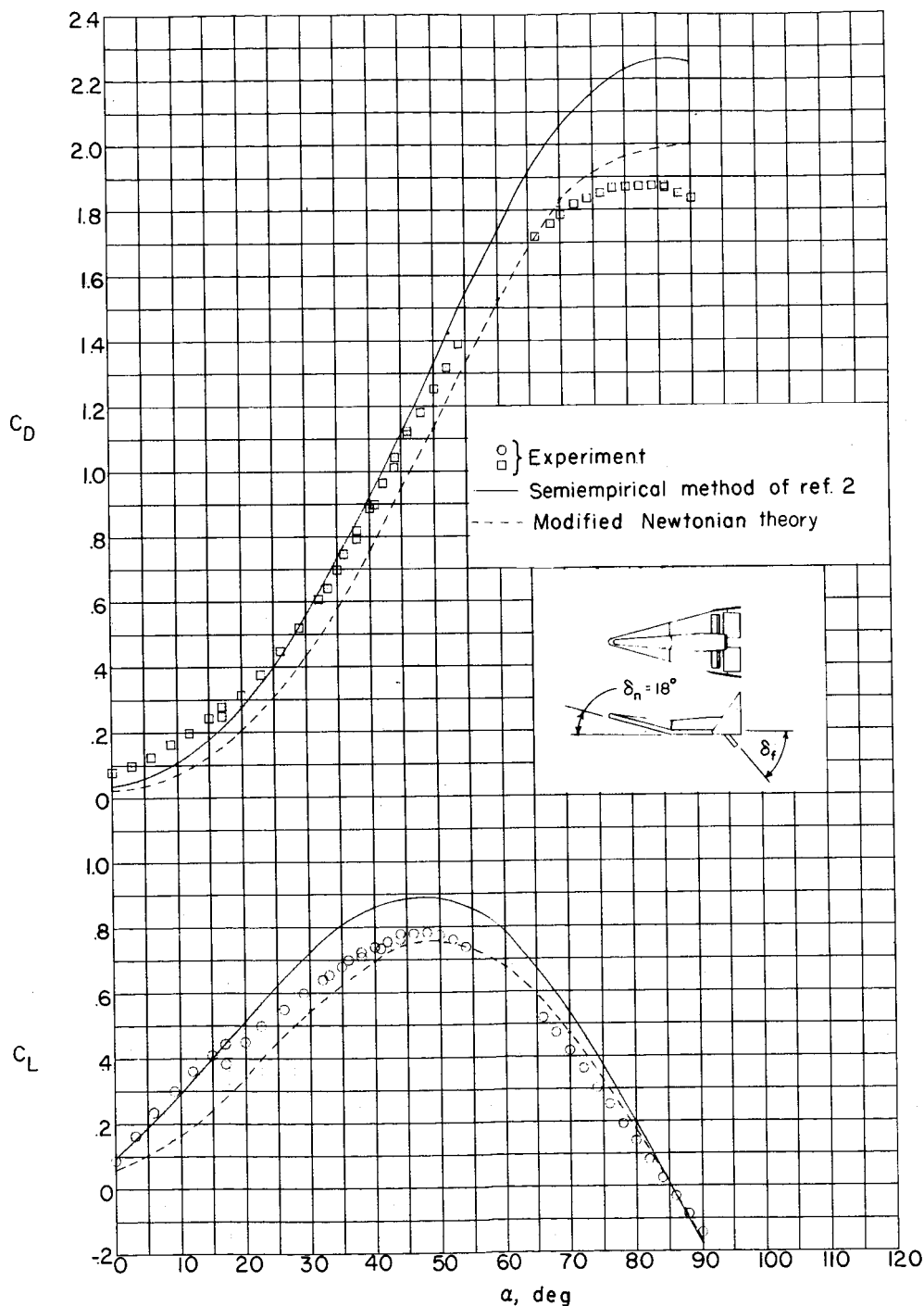
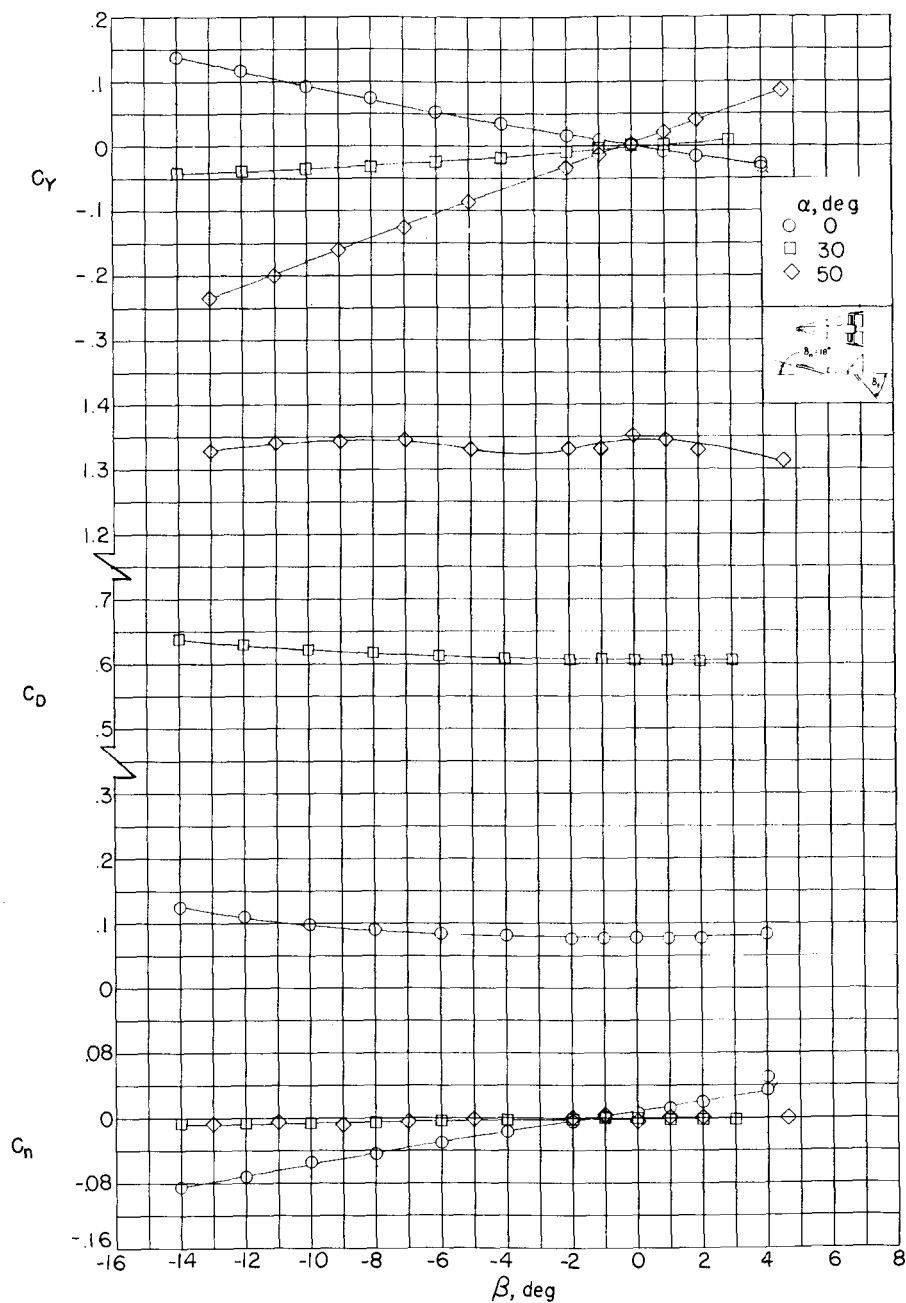


Figure 9.- Comparison of experimental  $C_L$  and  $C_D$  results of Model C (large tip fins;  $\delta = 0^\circ$ ) with theory.

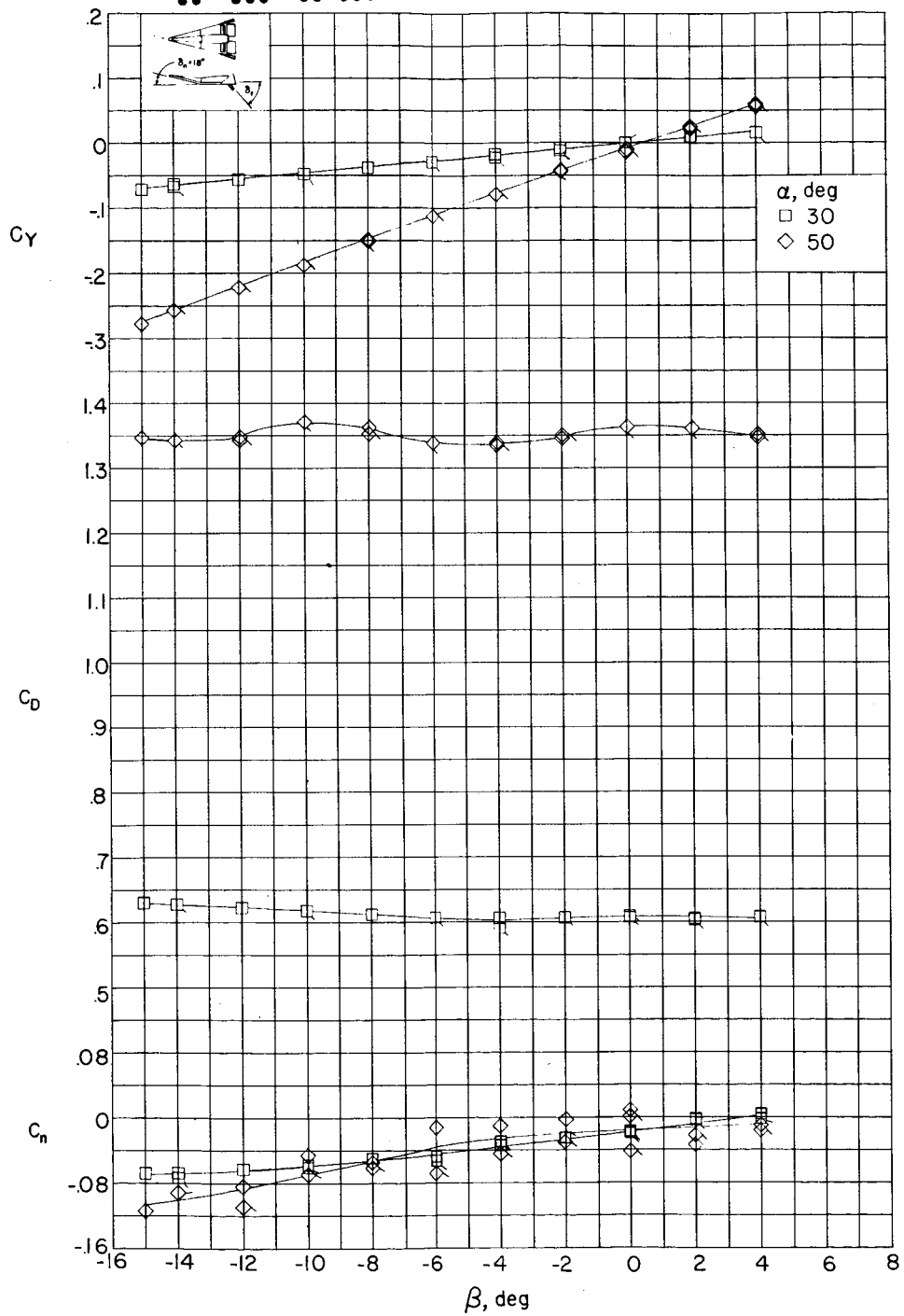
0344 0344 0344 0344



(a) Model C with large tip fins. (Flagged symbols denote check points.)

Figure 10.- Directional stability characteristics of model C with  $\delta_f = 0^\circ$ .

DECLASSIFIED



(b) Model C with small tip fins. (Flagged symbols denote check points.)

Figure 10.- Concluded.





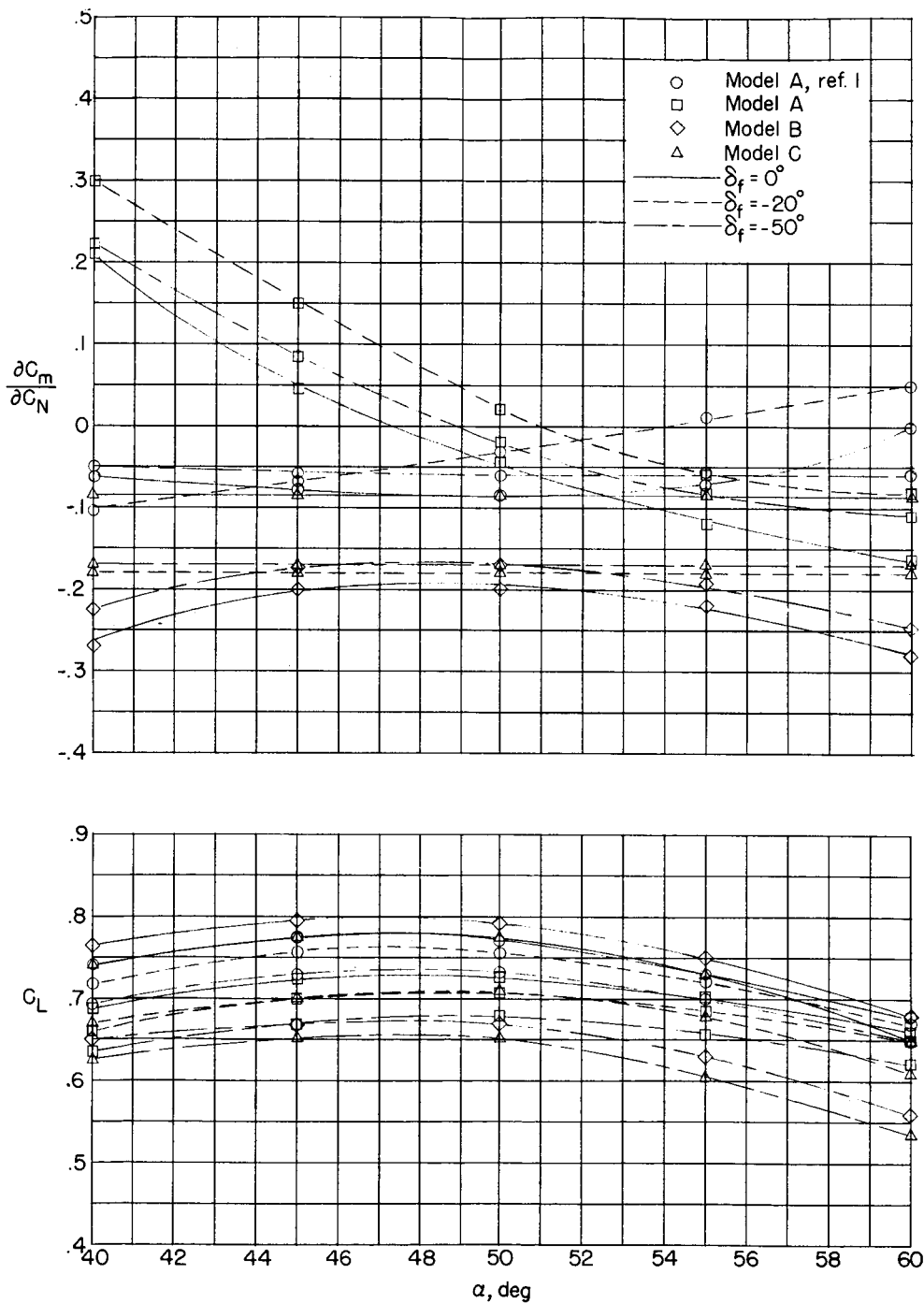


Figure 12.- Comparison of the effect of flap deflection on  $C_L$  and the longitudinal stability parameter for models A of reference 1, A, B, and C (with large tip fins).